Zeitschrift: Helvetica Physica Acta
Band: 61 (1988)
Heft: 5

Artikel: Neutron interferometric tests of quantum mechanics
Autor: Rauch, H.
DOI: https://doi.org/10.5169/seals-115964

Helvetica Physica Acta, Vol. 61 (1988) 589–610 0018–0238/88/050589–22$1.50 + 0.20/0

Neutron interferometric tests of quantum mechanics[1]

By H. Rauch

Atominstitut der Österreichischen Universitäten A-1020 Wien, Austria

(17. XII. 1987)

Abstract. Interferometers based on wavefront and amplitude division have been developed in the past. Most experiments have been performed with the perfect crystal neutron interferometer which provides widely separated coherent beams enabling new experiments in the field of fundamental nuclear- and solid state physics. A nondispersive sample arrangement and the difference between stochastic and deterministic absorption has been investigated. The verification of the 4π-symmetry of spinors and of the quantum mechanical spin-superposition experiment on a macroscopic scale are typical examples of interferometry in spin space. These experiments were continued with two resonance coils in the beams where the results showed that coherence persists, even if an energy exchange between the neutron and the resonator system occurs with certainty. A quantum beat effect was observed when slightly different resonance frequencies were applied to both beams. In this case, an extremely high energy sensitivity of 2.7×10^{-19} eV was achieved. Phase echo systems, experiments with chopped beams and multiplate interferometry are discussed as examples for forthcoming experiments. All the results obtained up until now are in agreement with the formalism of quantum mechanics and stimulate the discussion about the interpretation of this basic theory.

1. Introduction

Three different kinds of neutron interferometers have been tested in the past. The slit interferometer is based on wavefront division and provides long beam paths but only a very small beam separation [1, 2]. The perfect crystal interferometer is based on amplitude division and is now most frequently used due to its wide beam separation and its universal availability for fundamental-, nuclear- and solid state physics research [3, 4]. The interferometer based on grating diffraction is a recent development and has its main application for very slow neutrons [5]. A schematical comparison is shown in Fig. 1. The perfect crystal interferometer provides highest intensity and highest flexibility for beam handling.

In this article the development and the application of the perfect crystal interferometer is reviewed. The first successful test of such an interferometer happened in 1974 at our small 250 kW TRIGA-reactor in Vienna [3] (Fig. 2).

The perfect crystal interferometer represents a macroscopic quantum

[1]) Review presented at the Gwatt-Workshop, October 15–17, 1987.

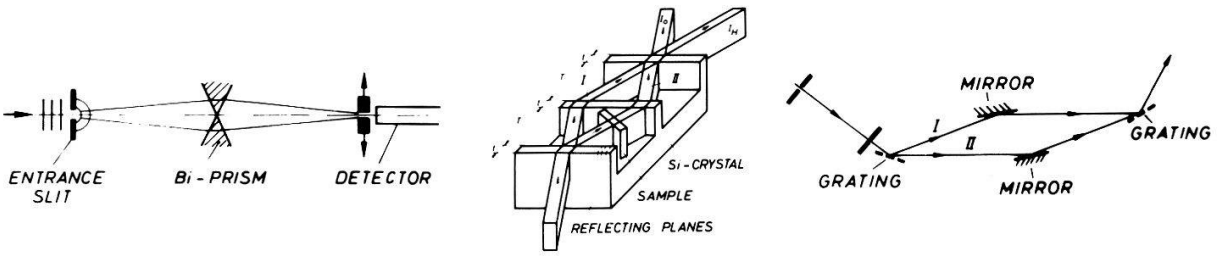

Figure 1
Scheme of a slit, a perfect crystal, and a grating interferometer.

device with characteristic dimensions of several centimeters. The basis for this kind of neutron interferometry is provided by the undisturbed arrangement of atoms in a monolithic perfect silicon crystal [3, 6]. An incident beam is split coherently at the first crystal plate, reflected at the middle plate and coherently superposed at the third plate (Fig. 1b). It follows immediately from general symmetry considerations that the wave functions in both beam paths, which compose the beam in the forward direction behind the interferometer, are equal ($\psi_0^I = \psi_0^{II}$), because they are transmitted-reflected-reflected (TRR) and reflected-reflected-transmitted (RRT), respectively. This method is based on Bragg diffraction from perfect crystals; therefore, the de Broglie wavelength of the neutrons is about 1.8 Å and their energy is about 0.025 eV.

The whole theoretical treatment of the diffraction process is based on the dynamical diffraction theory, which can also be found in the literature for the neutron case [7–10]. Inside the perfect crystal two wave fields are excited when the incident beam fulfills the Bragg condition, one of them having its nodes at the position of the atoms and the other in between them. Therefore, their vectors are slightly different ($k_1 - k_2 = 10^{-5}k_0$) and due to mutual interference processes, a rather complicated interference pattern is built up, which changes substantially over a characteristic length Δ_0 – the so-called Pandellösung length, which is of the order of 50 μm for an ordinary silicon reflection. To preserve the interference properties over the length of the interferometer, the dimensions of the monolithic

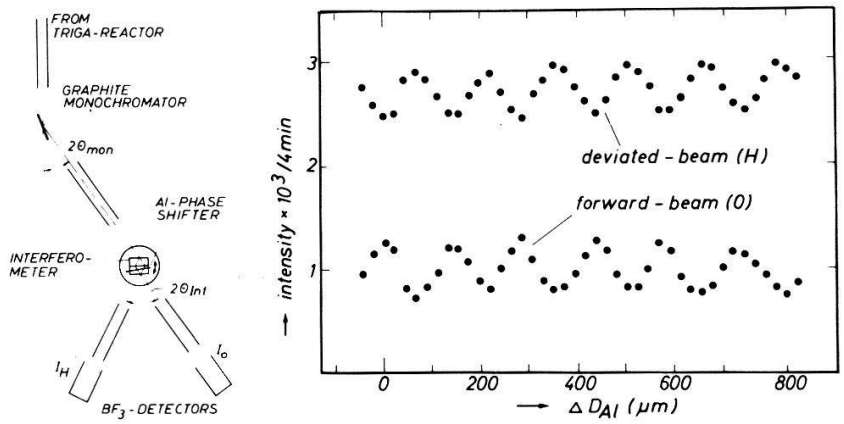

Figure 2
First observation of interference fringes with a perfect crystal interferometer [3].

system have to be accurate on a scale comparable to this quantity. Therefore, the whole interferometer crystal has to be placed on a stable goniometer table under conditions avoiding temperature gradients and vibrations.

A phase shift between the two coherent beams can be produced by nuclear, magnetic or gravitational interactions. In the first case, the phase shift is most easily calculated using the index of refraction [11, 12]:

$$n = \frac{k_{in}}{k_0} = 1 - \frac{\lambda^2 N}{2\pi}\sqrt{b_c^2 - \left(\frac{\sigma_r}{2\lambda}\right)} + i\frac{\sigma_r N\lambda}{4\pi} \tag{1.1}$$

(1.1) simplifies for weakly absorbing materials ($\sigma_r \to 0$) to

$$n = 1 - \lambda^2 \frac{Nb_c}{2\pi} \tag{1.2}$$

where b_c is the coherent scattering length and N is the particle density of the phase shifting material. As in ordinary light optics the change of the wave function is obtained as follows:

$$\psi \to \psi_0 e^{i(n-1)kD} = \psi_0 e^{-iNb_c\lambda D} = \psi_0 e^{i\chi}. \tag{1.3}$$

Therefore, the intensity behind the interferometer is given by

$$I_0 \propto |\psi_0^I + \psi_0^{II}|^2 \propto (1 + \cos\chi) \tag{1.4}$$

The intensity of the beam in the deviated direction follows from particle conservation:

$$I_0 = I_H = \text{const.} \tag{1.5}$$

Thus, the intensities behind the interferometer vary as a function of the thickness D of the phase shifter, the particle density N or the neutron wavelength λ.

Any experimental device deviates from the idealized assumptions made by the theory: the perfect crystal can have slight deviations from its perfectness, and its dimensions may vary slightly; the phase shifter contributes to imperfections by variations in its thickness and inhomogeneities; and even the neutron beam itself contributes to a deviation from the idealized situation because of its wavelength spread $\Delta\lambda$. Therefore, the experimental interference patterns have to be described by a generalized relation

$$I \propto A + B\cos(\chi + \phi_0) \tag{1.6}$$

where A, B and ϕ_0 are characteristic parameters of a certain set-up. It should be mentioned, however, that the idealized behaviour described by equation (1.4) can nearly be approached by a well balanced set-up [13]. The reduction of the contrast at high order results from the longitudinal coherence length which is determined by the wavelength spread of the neutron beam ($\Delta\chi_L = \lambda_0^2/\Delta\lambda$). This causes a change in the amplitude factor of equation (1.6) as ($B \to B\exp[-(\Delta\lambda/\lambda_0)^2\chi_0^2/2]$). The wavelength dependence of χ in equation (1.3) disappears in a special sample position where the surface of the sample is oriented

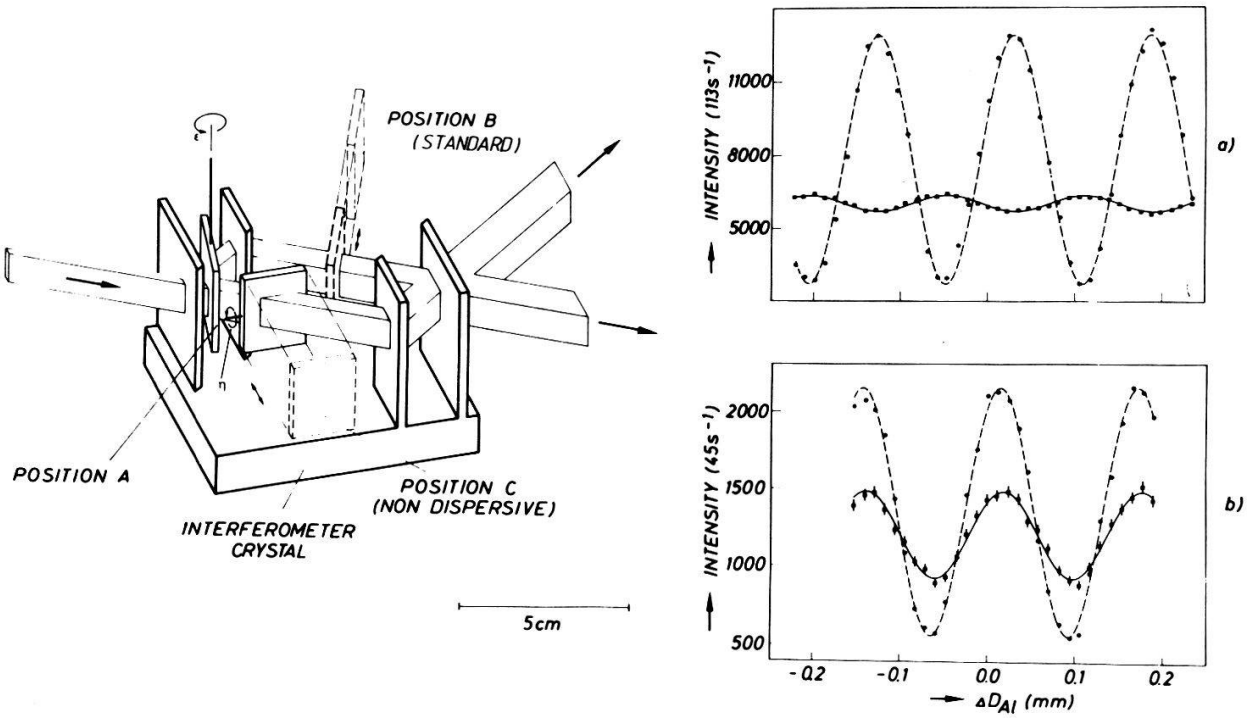

Figure 3
Interference pattern observed at high order ($m = 256$) with a dispersively (above) and a nondispersively arranged sample [14] (Dashed lines correspond to measurements at low order).

parallel to the reflecting planes and the path length through the interferometer becomes $D_0/\sin\theta_B$ and, therefore, the phase shift $\chi = -2d_{hkl}Nb_cD_0$ becomes independent of the wavelength. In this case the damping at high interference orders due to the wavelength spread does not appear as in the standard position. Related results of a recent experiment where the interference pattern in the 256 interference order have been measured in the dispersive and the nondispersive sample position are shown in Fig. 3. [14]. The much higher visibility of the interferences for the nondispersive sample arrangement is visible.

All the results of interferometric measurements, obtained up until now can be explained well in terms of the wave picture of quantum mechanics and the complementarity principle of standard quantum mechanics. Nevertheless, one should bear in mind that the neutron also carries well defined particle properties, which have to be transferred through the interferometer. These properties are summarized in Table 1 together with a formulation in the wave picture. Both particle and wave properties are well established and therefore, neutrons seem to be a proper tool for testing quantum mechanics with massive particles, where the wave-particle dualism becomes obvious.

All neutron interferometric experiments pertain to the case of self-interference, where during a certain time interval, only one neutron is inside the interferometer, if at all. Usually, at that time the next neutron has not yet been born and is still contained in the uranium nuclei of the reactor fuel. Although there is no interaction between different neutrons, they have a certain common history within predetermined limits which are defined, e.g., by the neutron

Table 1
Properties of the neutrons

PARTICLE PROPERTIES	
mass	$m_0 = 1.6749543(86) \cdot 10^{-24}$ g
spin	$s = \frac{1}{2}\hbar$
magnetic moment	$\mu = -1.91304308(54)\,\mu_K$
half live	$T_{1/2} = 641(8)$ s
electric charge	$q < 2.2 \cdot 10^{-20}$ e
electric dipol moment	$d < 4.8 \cdot 10^{-25}$ e cm
confinement radius	$R = 0.7$ fm
quark structure	$n = u - d - d$
kinematic relations	$\mathbf{p} = m\mathbf{v} \quad E = \frac{m\mathbf{v}^2}{2}$
WAVE PROPERTIES	
Compton wavelength	$\lambda_c = \frac{h}{mc} = 1.32 \cdot 10^{-13}$ cm
de Broglie wavelength	$\lambda_B = \frac{h}{mv} \simeq 1 \cdot 10^{-8}$ cm*)
coherence length	$\lambda_c = \lambda^2/\Delta\lambda \simeq 1 \cdot 10^{-6}$ cm*)
packet length	$\lambda_p = v \cdot \Delta t \simeq 1 \cdot 10^{0}$ cm*)
decay length	$\lambda_d = v \cdot T_{1/2} \simeq 2 \cdot 10^{8}$ cm*)
phase difference	$0 \leqslant \chi \leqslant 2\pi$

*) Values belong to thermal neutrons ($\lambda_B = 1.8$ A, $v = 2200$ m/s).

moderation process, by their movement along the neutron guide tubes, by the monochromator crystal and by the special interferometer set-up. Therefore, any real interferometer pattern contains single particle and ensemble properties together. In the following chapters typical experiments performed mainly by our group within the last 12 years will be presented.

2. Stochastic versus deterministic absorption

A certain beam attenuation can be achieved either by a semi-transparent material or by a proper chopper system. The transmission probability in the first case is defined by the absorption cross section σ_a of the material [$a = I/I_0 = \exp(-\sigma_a ND)$] and the change of the wave function is obtained directly from the complex index of refraction (equation (1.1)):

$$\psi \rightarrow \psi_0 e^{i(n-1)kD} = \psi_0 e^{i\chi} e^{-\sigma_a ND/2} = e^{i\chi}\sqrt{a}\psi_0 \tag{2.1}$$

Therefore, the beam modulation behind the interferometer is obtained in the following form

$$I_0 \propto |\psi_0^I + \psi^{II}|^2 \propto [(1+a) + 2\sqrt{a}\cos\chi] \tag{2.2}$$

On the other hand, the transmission probability of a chopper wheel or another shutter system is given by the open to closed ratio, $a = t_{\text{open}}/(t_{\text{open}} + t_{\text{closed}})$, and

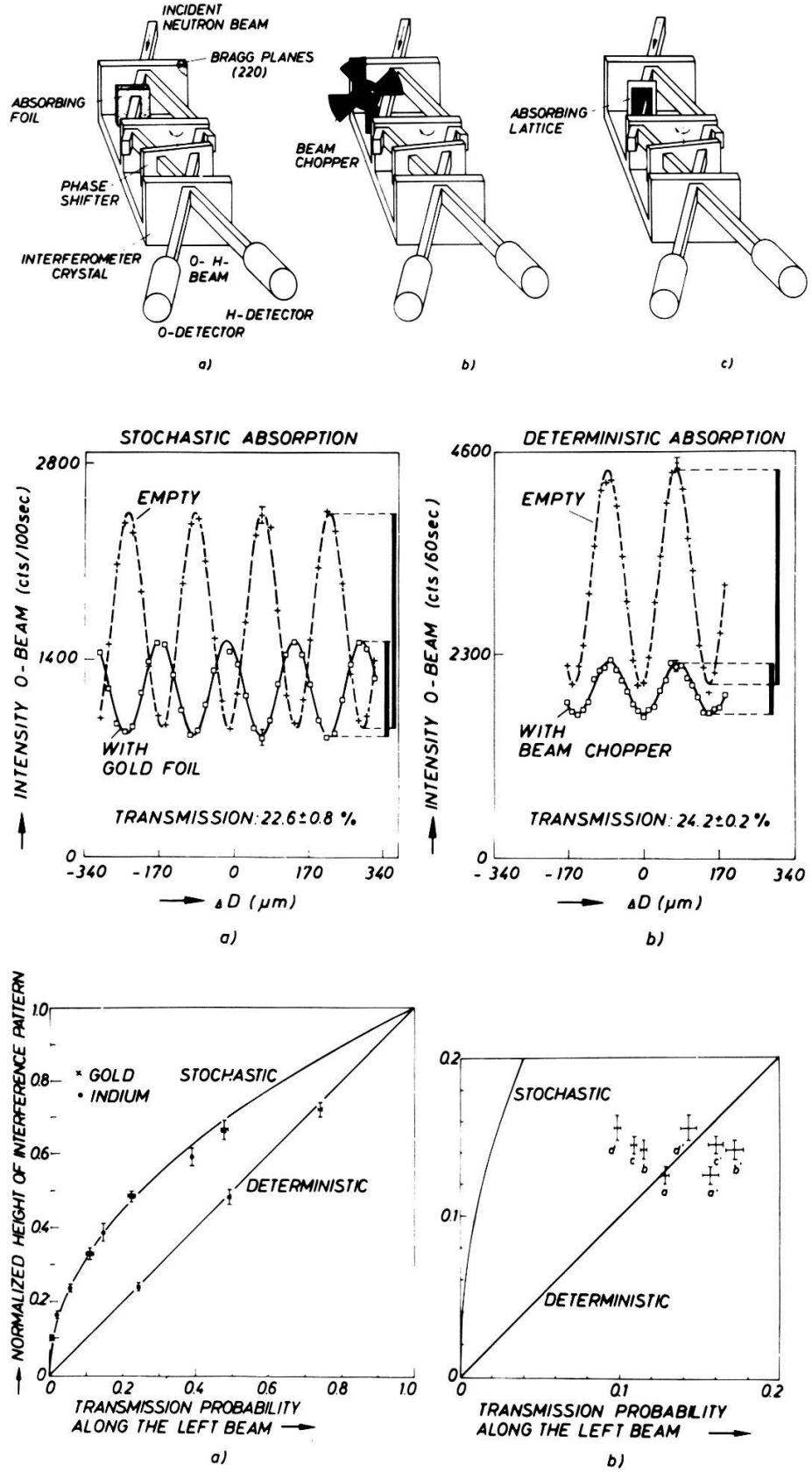

Figure 4
Sketch of the experimental arrangement for absorber measurements (above) (a) stochastic absorption, (b) deterministic absorption, (c) attenuation by a transmission grating. Typical results for stochastic and deterministic absorption (middle). Reduction of the contrast as a function of beam attenuation for different absorption methods (below). Individual points in (b) correspond to beam attenuation by the transmission grating [16].

one obtains after straightforward calculations

$$I \propto [(1-\alpha)\,|\psi_0^{II}|^2 + a\,|\psi_0^I + \psi_0^{II}|^2]$$
$$\propto [(1+a) + 2a\cos\chi] \tag{2.3}$$

i.e. the contrast of the interference pattern is proportional to $\sqrt{a}$, in the first case, and proportional to a in the second case, although the same number of neutrons has been observed in both cases. The absorption represents a measuring process in both cases because a compound nucleus is produced with an excitation energy of several MeV, which is usually deexcited by capture gamma rays. These can easily be detected by different means.

Figure 4 shows a typical result for the transmission probabilities near to $a = 0.25$ as well as the dependence of the normalized contrast on the transmission probability [15, 16]. The different contrast becomes especially obvious for low transmission probabilities where the interfering part of the interference pattern is distinctly larger than the transmission probability through the semitransparent absorber sheet. The region between the linear and the square root behaviour can be achieved by very narrow chopper slits or by a narrow transmission lattice, where one starts to loose information of through which individual slit the neutron went. The critical slit width is connected to the Pendellösung length and to the fact that certain neutrons become "labeled" neutrons due to slit diffraction which makes a separate detection possible in principle.

3. 4π-symmetry of spinors

The magnetic interaction is caused by the dipole coupling of the magnetic moment of the neutron $\boldsymbol{\mu}$ to a magnetic field $\mathbf{B}$ ($H = -\boldsymbol{\mu}\mathbf{B}$). Therefore, the propagation of the wavefunction is given by

$$\psi \rightarrow \psi_0 e^{-i(Ht/\hbar)} = \psi_0 e^{-i(\boldsymbol{\mu}\mathbf{B}t/\hbar)} = \psi_0 e^{-i\boldsymbol{\sigma}\boldsymbol{\alpha}/2} = \psi(\alpha) \tag{3.1}$$

where $\boldsymbol{\alpha}$ represents a formal description of the Larmor rotation angle around the field $\mathbf{B}$ ($\alpha = (2\mu/\hbar)\int B\,\mathrm{d}t = (2\mu/\hbar v)\int B\,\mathrm{d}s$). This wave function shows the typical 4π-symmetry of a spinor

$$\psi(2\pi) = -\psi(0)$$
$$\psi(4\pi) = \psi(0) \tag{3.2}$$

whereas 2π-symmetry exists only for the expectation values

$$|\psi(2\pi)|^2 = |\psi(0)|^2 \tag{3.3}$$

The 4π-periodicity becomes visible in interferometer experiments, as predicted theoretically [17–19], and has been verified experimentally in early neutron interferometric experiments [20, 21], where the intensity for unpolarized incident

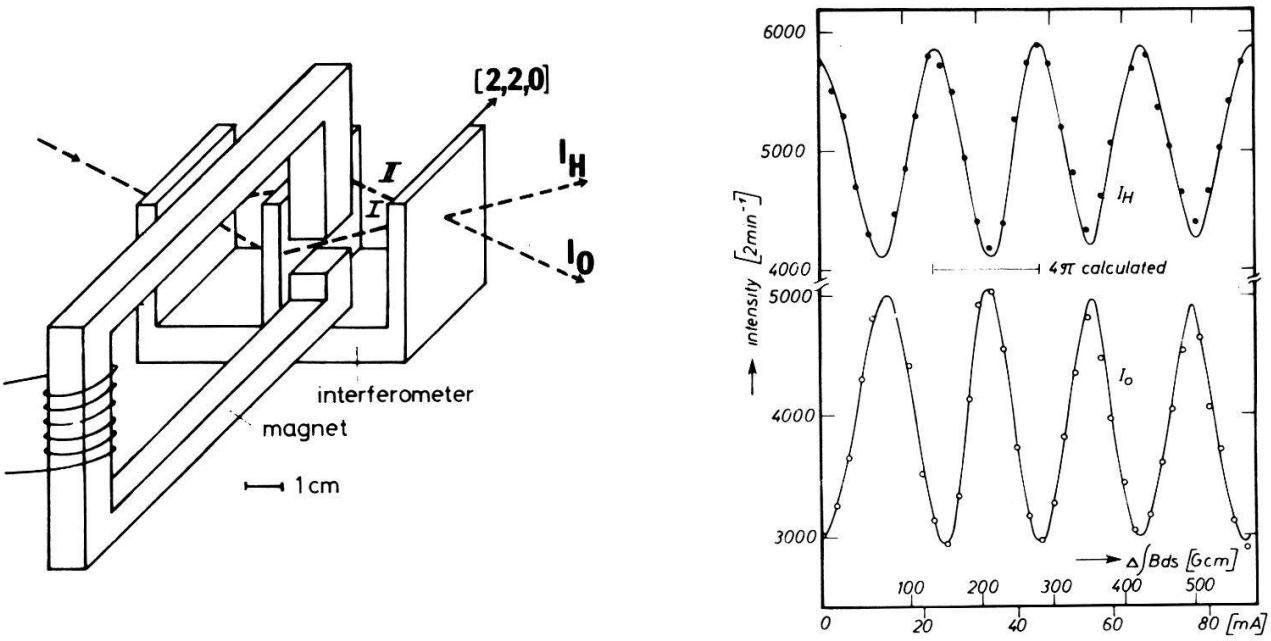

Figure 5
First observation of the 4π-symmetry factor of spinors [20].

neutrons was found to be

$$I_0 \propto |\psi(0) + \psi(\alpha)|^2 \propto \left(1 + \cos\frac{\alpha}{2}\right) \tag{3.4}$$

The results of the first related experiment are shown in Fig. 5. These results are widely debated in the literature. It should be mentioned, that this 4π-symmetry can always be attributed to real rotations in the case of fermions [22, 23]. Today, the most precise value for the periodicity factor is $\alpha_0 = 715.87 \pm 3.8$ degrees [24]. This value provides only a small margin for speculation about SU(2)-symmetry breaking, but a new and more precise determination of α_0 is recommended. The 4π-periodicity effect has been observed for unpolarized as well as polarized neutrons, which demonstrates the intrinsic feature of this phenomenon and the self-interference properties involved in this kind of experiments. New attention should be drawn to an interferometric observation of the Berry phase [25] which represents a topological phenomenon and is therefore of central interest too.

4. Spin state interferometry

In this case the polarization vector can be influenced differently in the two coherent beam paths and these beams can be superposed at the end of the interferometer. The principles of these experiments and the most important results are summarized in Fig. 6 [26, 27]. More experimental details can be found in these references. There is a marked difference between the action of a static flipper and a resonance flipper, which has to be discussed in more detail.

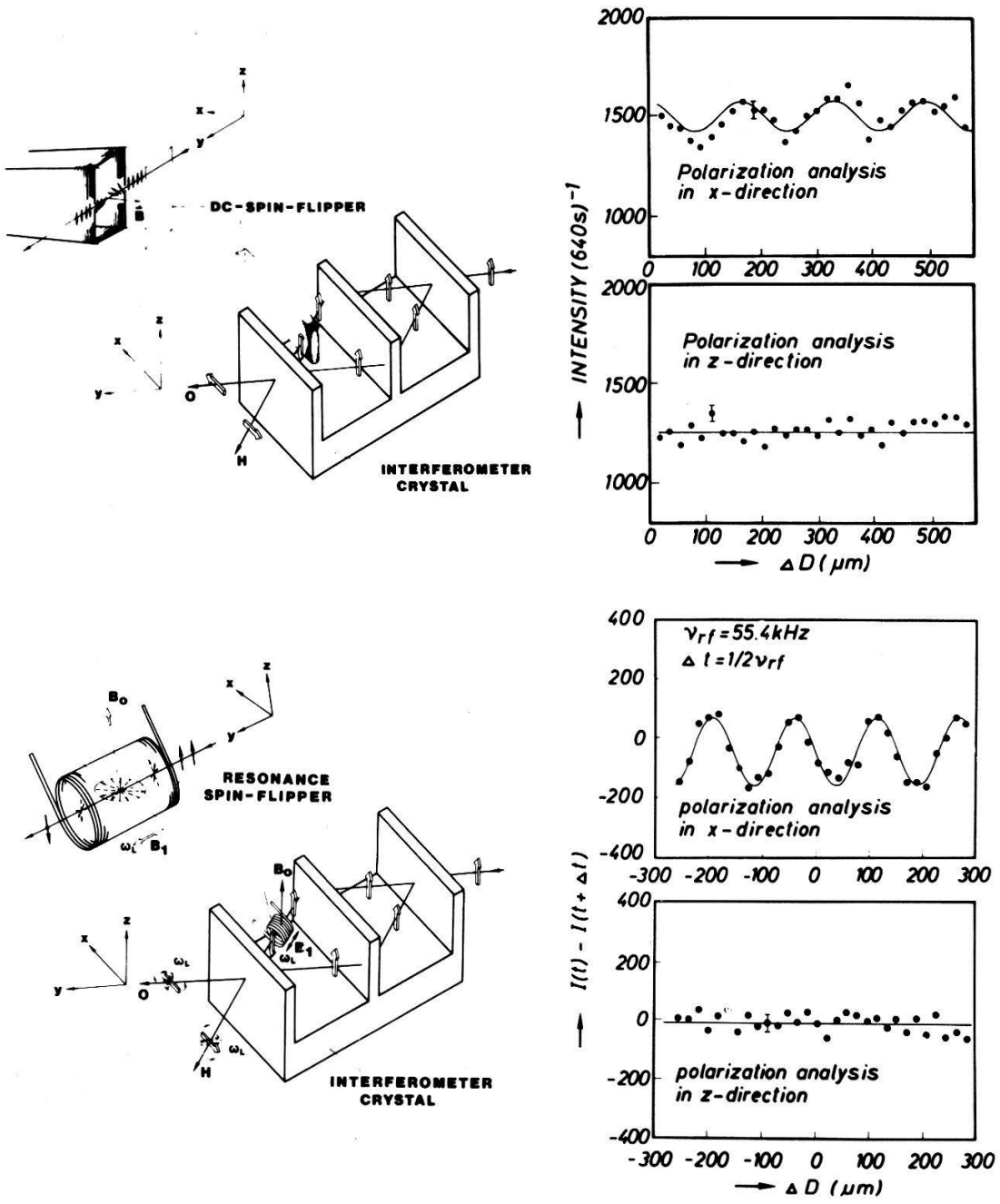

Figure 6
Sketch of the static (above) and the time-dependent (below) spin superposition experiment with characteristic results [26, 27].

In the first case (static flipper) the wave function is changed by the flipper according to equation (3.1), which has to be applied for polarized incident neutrons:

$$\psi \rightarrow e^{i\chi} e^{-i\sigma\alpha/2} |z\rangle = e^{i\chi} e^{-i\sigma_y \pi/2} |z\rangle = -i\sigma_y e^{i\chi} |z\rangle = e^{i\chi} |-z\rangle \tag{4.1}$$

The rotation of the polarization vector around the y-axis has been postulated to be π [28]. Thus, two wave functions with opposite spin directions are superposed at the third plate

$$\psi \propto (|z\rangle + e^{i\chi} |-z\rangle \tag{4.2}$$

which corresponds to the situation proposed by Wigner [29] in 1963 to verify the quantum mechanical spin superposition law. In this case the intensities in the O— and H— beams are equal, and the beams are polarized in the (x, y)-plane, i.e. perpendicular to both the initial spin directions. The angle of the polarization in the (x, y)-plane is given by the nuclear phase shift.

$$\mathbf{P}_0 = \frac{\langle \psi | \boldsymbol{\sigma} | \psi \rangle}{I_0} = \begin{pmatrix} \cos \chi \\ \sin \chi \\ 0 \end{pmatrix} \tag{4.3}$$

Thus, a pure initial state is transferred to a pure final state which is different to both states existing before superposition. The interference pattern appears only, if a polarization analysis is performed in the $|x\rangle$- or in the $|y\rangle$-direction. If the analyzer is set in the $|z\rangle$- (or $|-z\rangle$)-direction, no intensity modulation is observed.

The second version of the spin superposition experiment was performed with a Rabi-type resonance flipper which is also commonly used in polarized neutron physics. This kind of interaction is time-dependent and, in addition to the spin-inversion, an exchange of the resonance energy $E_{HF} = \hbar\omega_r$ occurs between the neutron and the resonator system, which has to be considered in the interferometric experiment. This energy exchange was observed in a separate experiment, where the energy resolution ΔE of the apparatus was better than the Zeeman energy splitting ($\Delta E < E_{HF}$) [30]. This experiment was performed according to a proposal of Drabkin and Zhitnikov [31]. For a complete spin reversal the frequency of the field has to match the resonance condition and the amplitude B_1 has to fulfill the relation $|\mu| B_1 l/\hbar v = \pi$, where l is the length of the coil. Oscillating fields are used instead of purely rotational fields and, therefore, only one component contributes to the resonance which causes a slight shift of the resonance frequency from the Larmor frequency $\omega_L = 2|\mu| B_0/\hbar$ due to the Bloch–Siegert effect ($\omega_r = \omega_L[1 + (B_1^2/16B_0^2)]$) [32, 33]. Thus, the wave function of the beam with the flipper changes according to

$$\psi \rightarrow e^{i\chi} e^{i(\omega - \omega_r)t} | -z \rangle. \tag{4.4}$$

Therefore, a spin-up and a spin-down state are superposed at the position of the third plate. The final polarization of the beam in the forward direction is given by

$$\mathbf{P} = \begin{pmatrix} \cos(\chi + \omega_r t) \\ \sin(\chi + \omega_r t) \\ 0 \end{pmatrix} \tag{4.5}$$

and lies again in the (x, y)-plane but now rotates within this plane with the resonance (Larmor) frequency without being driven by a magnetic field. A stroboscopic method was needed for the observation of this effect. The direction of the polarization in the (x, y)-plane depends on the status (phase) of the resonance field and, therefore, has to be measured synchronously with this phase.

The observed interference pattern (Fig. 6) demonstrates that coherence

persists, although a well defined energy exchange between the neutron and the apparatus exists. Thus, an energy exchange is not automatically a measuring process. As we will see later on, the exchanged photon cannot be used for a quantum nondemolitian measurement. In our experiment, the following argument based on different uncertainty relations can be used: Firstly, one single absorbed or emitted photon of the resonator cannot be detected because of the photon number-phase uncertainty relation, which can be written in the form [34, 35]

$$(\Delta N)^2 \frac{(\Delta S)^2 + (\Delta C)^2}{\langle S\rangle^2 + \langle C\rangle^2} \geqslant \frac{1}{4}, \tag{4.6}$$

where S and C can be expressed by the creation and annihilation operators, $C = (a_- + a_+)/2$ and $S = (a_- - a_+)/2i$, whose matrix elements couple coherent Glauber states. For our purpose this relation can be used in its simpler form

$$\langle \Delta N^2\rangle \langle \Delta\theta^2\rangle \geqslant \tfrac{1}{4}. \tag{4.7}$$

The uncertainty of the photon number of the resonator is minimized for a coherent state resonator by $\Delta N \simeq \sqrt{\langle N\rangle}$ [36] and, therefore, the lower limit for the phase uncertainty becomes $\Delta\theta \simeq 1/(2\sqrt{\langle N\rangle})$. Because in this kind of spin-superposition experiment the phase determination of the flipper field is required to be better than $\theta \leqslant \frac{1}{2}$ for the stroboscopic method, it is impossible to observe a single absorbed or emitted photon ($\Delta N \geqslant 1$).

A second version of the beam path detection may be based on the observation of the energy change of the neutron. This can only be achieved, if the energy resolution of the instrument fulfills the relation $\Delta E \leqslant 2\mu B_0$. On the other hand, the stroboscopic measuring method requires time channels $\Delta t \leqslant \frac{1}{2}\nu_{HF} = h/4\,|\mu|\,B_0$, which provides another constraint on the experiment. Both conditions cannot be fulfilled with respect to the energy-time uncertainty relation concerning the beam parameters $\Delta E \Delta t \geqslant \hbar/2$. Therefore, we conclude that a simultaneous detection of the beam path through the interferometer and of the interference pattern remains impossible.

It has been argued by Vigier's group [37, 38], that new information about the particle-wave duality can be obtained with resonator coils in both coherent beams. They calculated the quantum potential and the beam trajectories [39, 40] within the frame of the causal stochastic view of quantum mechanics (Fig. 13). Unfortunately the results of these calculations are identical with the results of ordinary quantum mechanics and, therefore, to decide between both points of view remains an epistemological problem. The corresponding experiments will be discussed in the next chapter.

5. Double coil experiments

The experimental arrangement for the double coil experiment is shown in Figure 7 [41, 42]. The final polarization lies in the $|-z\rangle$ direction and the energy

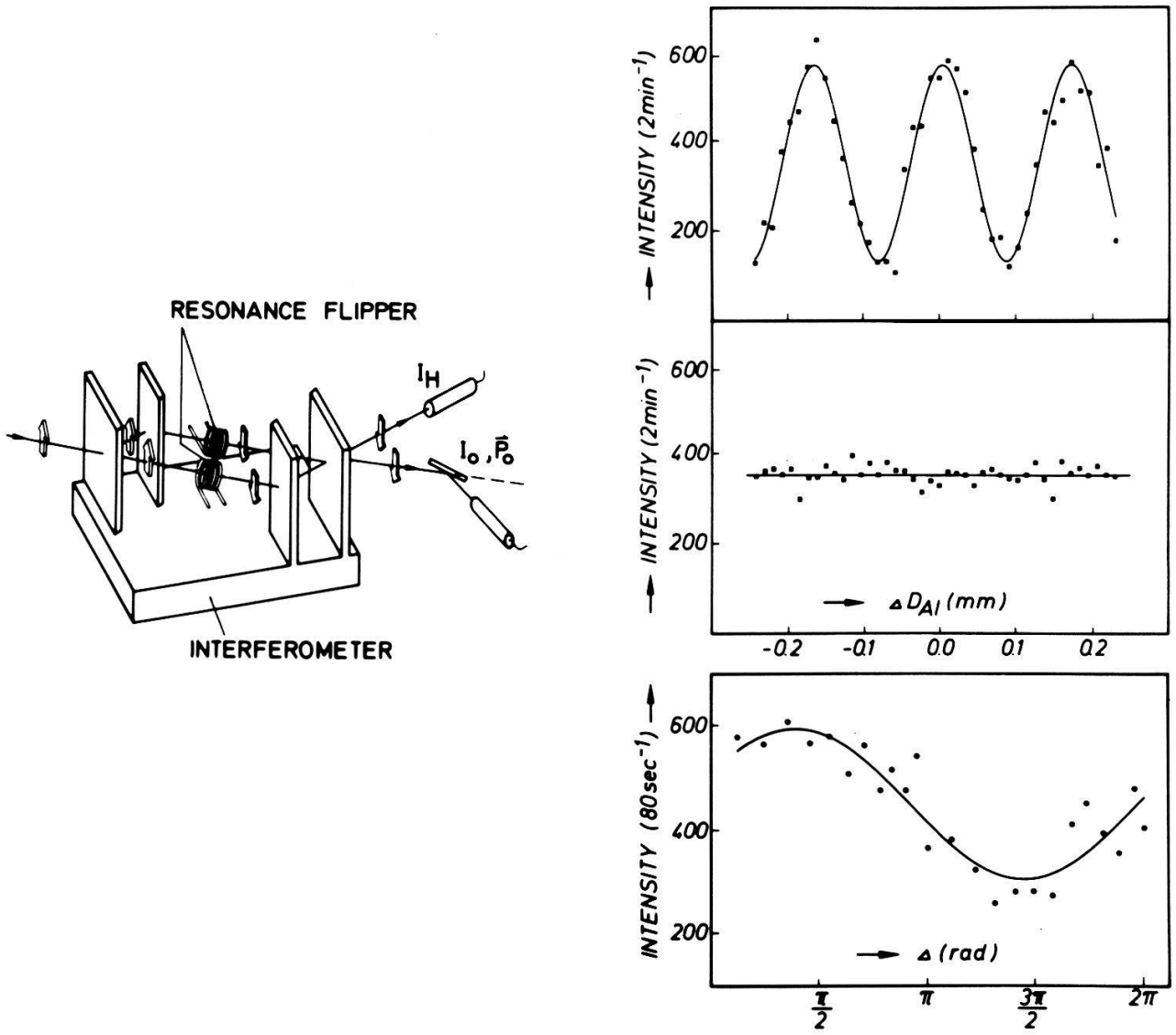

Figure 7
Sketch of the double resonance coil experiment (right) and results of the double coil experiments (left) [41, 42]. Above: Synchronous flipper fields with $\nu_r = 71.90$ kHz (equation 4.1). Middle: Two slightly fluctuating independent flipper fields with $\nu_r = 71.92 \pm 0.02$ kHz (equation 4.3). Below: Interference pattern as a function of the phase shift Δ between both flipper fields at $\nu_r = 71.90$ kHz (equation 4.4).

transfer $\hbar\omega_r$ can be smaller or larger than the energy resolution ΔE because this information can not be in any way associated with a beam path detection. The lay-out of the experiment followed the proposal of Vigier's group [37, 38]. According to our previous considerations the change of the wave functions with the resonance flippers turned to the resonance frequency can be written for polarized incident neutrons ($|z\rangle$) and for different modes of operation as follows.

a) Both flippers are operated synchronously without a phase shift between the flipper fields:

$$\psi \rightarrow e^{i(\omega-\omega_r)t}\,|-z\rangle + e^{i\chi}e^{i(\omega-\omega_r)t}\,|-z\rangle \tag{5.1}$$

This results in an intensity modulation

$$I_0 \propto 1 + \cos \chi \tag{5.2}$$

which is independent of the flipper fields.

b) Both flippers are operated synchronously with a distinct phase relation Δ:

$$\psi_0 \rightarrow e^{-i(\omega-\omega_r)t} \mid -z\rangle + e^{i\chi} e^{i\Delta} e^{i(\omega-\omega_r)t} \mid -z\rangle. \tag{5.3}$$

In this case, the intensity modulation is given by

$$I_0 \propto 1 + \cos(\chi + \Delta). \tag{5.4}$$

c) Both flippers are operated asynchronously with statistically fluctuating phase differences $\Delta(t)$ which average out during the measuring interval. Then

$$I_0 \propto \text{const.} \tag{5.5}$$

It should be mentioned in this context, that even in this case, coherence phenomena can be observed if a stroboscopic investigation is performed ($I_0 = I_0(\Delta)$).

The results of these related experiments are shown in Fig. 7. Complete agreement with the theoretical predictions is found. The interference properties are preserved, although an energy exchange $\hbar\omega_r$ certainly takes place. Only quanta within a narrow energy band around $\hbar\omega_r$ and no others are excited inside the flipper resonator. Therefore, one could believe that the spin flip and the energy transfer process to the neutron occurred inside one of the two coils, which would demonstrate that the neutron has chosen one of the two possible paths. But even this rather weak statement would require the concept of pilot waves, quantum potentials, etc., leading immediately to questions about the interpretation of quantum mechanics, which are not the subject of this article.

6. Macroscopic quantities in uncertainty relations

By means of perfect crystal neutron optics the resolution in momentum or energy space can be increased to such an extent, that the conjugate quantities each macroscopic dimensions.

Firstly, the perfect crystal can be envisaged as a very narrow collimator, whose angular divergence is roughly given by the ratio of the lattice constant divided by the thickness of the crystal (d_{hkl}/t). This feature becomes visible in multiple Laue-rocking curves, where the convolution of the individual reflection curves exhibits a very narrow central peak [43, 44] which has similarities to the diffraction focussing effect first treated for X-rays [45]. The individual reflection curves are well known from dynamical diffraction theory and can be written as [7, 8]

$$P(y) = \frac{\sin^2 \sqrt{A(1+y^2)}}{1+y^2} \tag{6.1}$$

where A is a reduced quantity related the thickness of the perfect crystal and y describes the deviation from the exact Bragg angle. At the same time, a narrow incident beam is spread out across the whole Borrmann fan, whose dimension at the exit is given by the thickness (t) of the crystal plates as $2t \cdot tg\theta_B$. The rapid variation of the intensity across the reflection curve or the Borrmann fan (Pendellösung fringes) is caused by the rapid variation of the phases of the excited waves inside the crystal. The corresponding rocking curves are given by the convolution of such fine structured curves. They can also be interpreted as self-correlation functions, which can be connected with the uncertainty relations [46]. The analytical form of the central peak of these multiple Laue rocking curves can be written as [47]

$$I_p \propto \frac{J_1(2Ay)}{Ay}. \tag{6.2}$$

The width at half maximum is given by

$$\delta\theta = 0.7\frac{d_{hkl}}{t} \tag{6.3}$$

which is of the order of several thousandths of a second and of arc. The related momentum uncertainty ($\Delta k = k\delta\theta$) is of the order of cm^{-1} and, therefore, Δx in the space-momentum uncertainty relation becomes of the order of cm. The formulas for the triple case Laue rocking curves and for various other contributions to the rocking curves can be found in the literature [47].

The experiments have been performed with monolithic multiplate systems by rotating a wedge shaped material around the beam axis; this provides a proper control of small beam deflections in the horizontal plane, which is the only sensitive plane for perfect crystal reflections. This deflection is given by the properties of the material, by the angle β of the wedge and by the rotation angle α around the beam axis

$$\delta = \frac{Nb_c\lambda^2}{\pi} tg\left(\frac{\beta}{2}\right) \sin\alpha \tag{6.4}$$

The broadening of the central peak due to the insertion of a macroscopic slit is shown in Fig. 8 [48]. More recently measurements with macroscopic transmission lattices have shown similar results. Although the wavelength of the neutrons is smaller than the width of the slit, by a factor of about 10^8 the broadening becomes visible due to the high angular resolution of such systems. This can also be understood by the large transversal coherence length of the beam across the whole Borrmann fan ($2t \cdot tg\theta_B$).

As an alternative to the high momentum resolution discussed before, an extremely high energy resolution can be achieved by a slight modification of the double coil experiment described in chapter 5. If the frequencies of the two coils are chosen to be slightly different, the energy transfer becomes different too ($\Delta E = \hbar(\omega_{r1} - \omega_{r2})$). The frequency difference can be made very small, if high

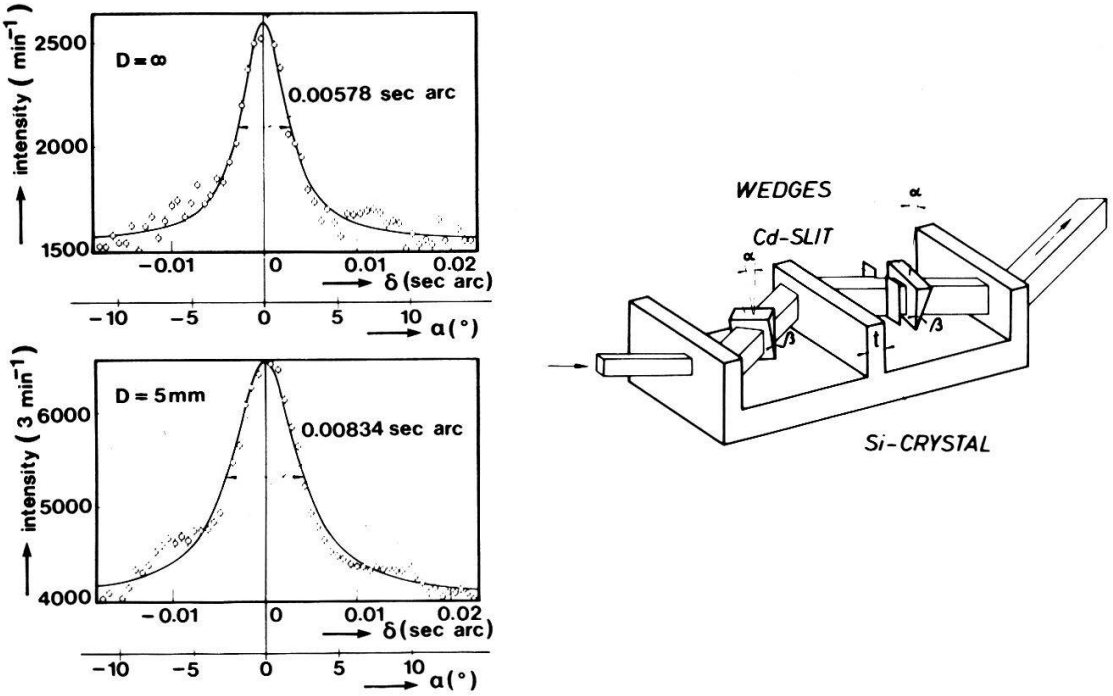

Figure 8
Experimental arrangement for the observation of triple Laue rocking curves and broadening of the narrow central peak due diffraction from a slit with a width of 5 mm [48].

quality synthesizers are used for the field generation. The flipping efficiencies for both coils are always very close to 1 (better than 0.99). Now, the wave functions change according to

$$\psi \rightarrow e^{i(\omega-\omega_{r1})t} \mid -z\rangle + e^{i\chi} e^{i(\omega-\omega_{r2})t} \mid -z\rangle \tag{6.5}$$

Therefore, the intensity behind the interferometer exhibit a typical quantum beat effect, given by

$$I \propto 1 + \cos\left[\chi + (\omega_{r1} - \omega_{r2})t\right] \tag{6.6}$$

Thus, the intensity behind the interferometer oscillates between the forward and deviated beam without any apparent change inside the interferometer [41, 42]. The time constant of this modulation can reach a macroscopic scale which is again correlated to an uncertainty relation $\Delta E\, \Delta t \leqslant \hbar/2$. Figure 9 shows the result of an experiment, where the periodicity of the intensity modulation, $T = 2\pi/(\omega_{r1} - \omega_{r2})$, amounts to $T = (47.90 \pm 0.15)s$ caused by a frequency difference of about 0.02 Hz. This corresponds to a mean difference of ΔE energy transfer between the two beams, $E = 8.6 \times 10^{-17}$ eV, and to an energy sensitivity of 2.7×10^{-19} eV, which is better by many orders of magnitude than that of other advanced spectroscopic methods. This high resolution is strongly decoupled from the monochromaticity of the neutron beam, which was $\Delta E_B = 5.5 \times 10^{-4}$ eV around a mean energy of the beam $E_B = 0.023$ eV in this case. It should be mentioned, that the result can also be interpreted as being the effect of a slowly varying phase $\Delta(t)$ between the two flipper fields (see equation 5.4), but the more physical description is based on the argument of a different energy transfer. The extremely

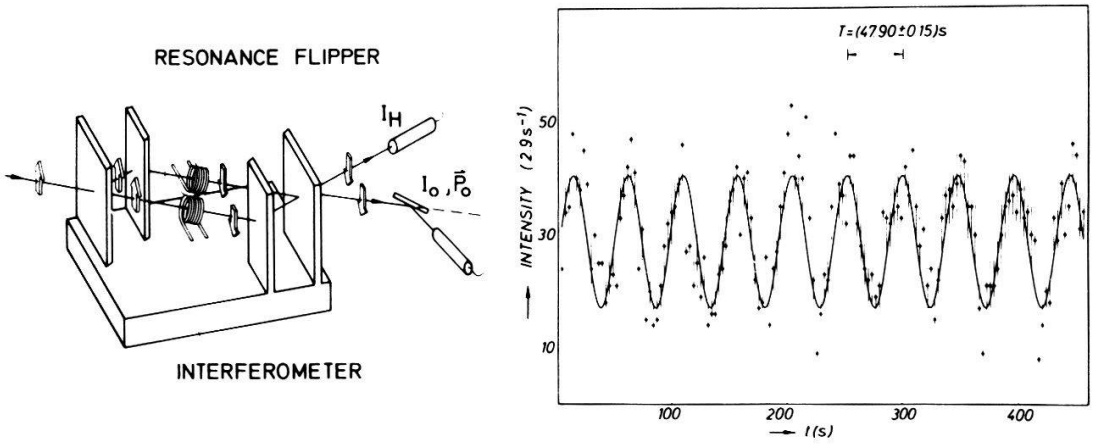

Figure 9
Quantum beat effect observed when the frequencies of the two flipper coils differ by about 0.02 Hz around 71.89979 kHz [42].

high resolution may be used for fundamental nuclear and solid state physics applications.

An intrinsic lower limit for the energy width ΔE_i of the neutron beam exists which is caused by its lifetime, $\tau = 925$ s. According to $\Delta E_i \tau \geqslant \hbar/2$, $\Delta E_i = 3.5 \times 10^{-24}$ eV. The decay appears in both beam paths and contributes an attenuation factor $\exp(-t/\tau) = \exp(-l\tau/v)$ which is similar to those discussed in Chapter 2.

7. Experiments in progress or in preparation

We feel that most of the fundamental experiments for testing quantum mechanics by neutron interferometry have already been performed. There remain possibilities for more accurate repetitions of these experiments under even better conditions which could produce spectacular results at any time. In addition, there may be new experiments, which could push the development of advanced neutron optics further. Some examples of such experiments will be discussed below:

(*a*) *Phase echo system*

Such systems are similar to spin echo systems known in advanced neutron spectroscopy [49], but use the phase of the wave function instead of the Larmor precession angle as the measurable quantity [50]. The interference pattern disappears, if the longitudinal shift of the wave packets due to a phase shifter becomes larger than the longitudinal coherence length of the beam ($\chi \cdot \lambda/2\pi > \lambda^2/\Delta\lambda$ see also Fig. 3). This behaviour has been observed experimentally [51, 52]. By applying an opposite phase shift in the same beam, or the same phase shift in the second beam of the interferometer, the smeared interference pattern can be recovered to full contrast, shown schematically in Fig. 10. Such experiments can demonstrate, that a phase information can exist although the measured signal looks like a statistical mixture. The coherence properties can be recovered, if a proper measuring method is applied. This method will establish a new horizon if

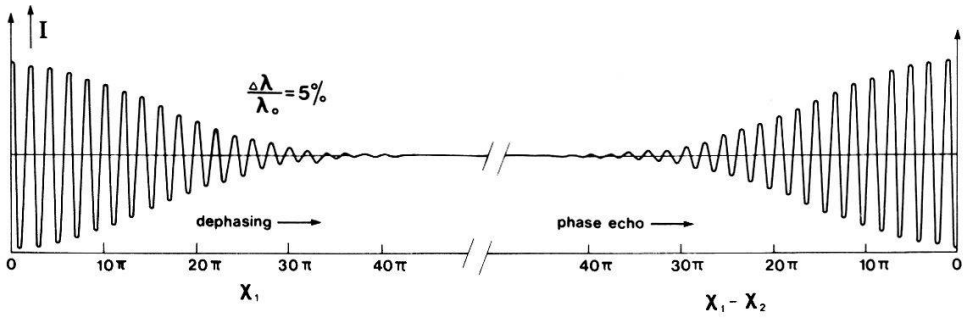

Figure 10
Principle of a phase echo system [50].

combined with multiplate interferometry (part (c)), where interference properties of a dephased beam can be recovered in the following interferometer loops.

(*b*) *Pulsed beam interferometry*

It could be argued, that there is always an overlap of wave functions in a stationary situation (or at least of plane wave components of the wave packet from both beam paths) at the position of the beam splitter and at the place of superposition. This can be avoided by using a chopper which produces bursts, whose lengths are smaller than the dimension of the interferometer (Fig. 11). The known spatial spreading of the wave function of matter waves

$$[\Delta x(t)]^2 = [\Delta x(0)]^2 + \left[\frac{(\hbar/2m)t}{\Delta x(0)}\right]^2 \tag{7.1}$$

has no influence on the interference properties for all practical situations, where the length of the bursts Δx are much larger than the coherence length, $\lambda^2/\Delta\lambda$. Nevertheless, such experiments will make the discussion about the collapse of the wave field in the case of an absorber (see Chapt. 2) more profound and new types of delayed choice experiments will become feasible where the decision about

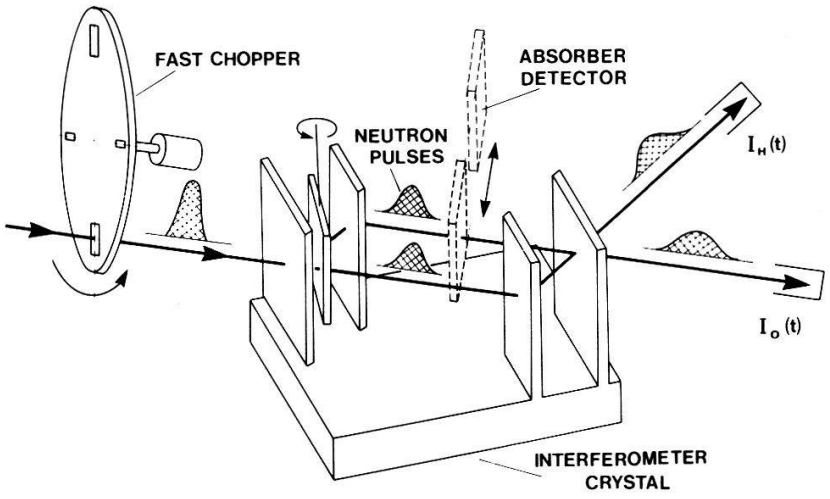

Figure 11
Sketch of the apparatus for interference experiments with pulsed beams.

interference or beam path detection can be made after the burst has passed the beam splitter.

(c) *Multiplate interferometry*

A five plate interferometer is shown in Fig. 12. In this set-up different interferometer loops are linked together by common beam paths. The theoretical description follows the formalism developed for the standard triple plate case [9, 10], but the expected interference properties show some new features, which do not exist for the standard interferometer. The whole theoretical description follows the treatment for the X-ray case [53, 54]; here we refer to a four plate interferometer and specify averaged intensities of the interfering beams behind this device:

$$\begin{aligned} I_3 &= K_2[3 + 2\cos(\chi_A + \chi_B) + 2\cos\chi_A + 2\cos\chi_B] \\ I_4 &= K_1 + 2K_3 - 2K_2[\cos(\chi_A + \chi_B) + \cos\chi_B] + 2K_3\cos\chi_A \\ I_5 &= 2K_2 + K_4 + 2K_2\cos(\chi_A + \chi_C) - 2K_3[\cos\chi_A + \cos\chi_C] \\ I_6 &= K_1 + 2K_3 - 2K_2[\cos(\chi_A + \chi_C) + \cos\chi_A] + 2K_3\cos\chi_C \end{aligned} \tag{7.2}$$

with

$$K_1 = \frac{417\pi}{1048}, \qquad K_2 = \frac{79\pi}{1048}, \qquad K_3 = \frac{65\pi}{1048}, \qquad K_4 = \frac{175\pi}{1048}.$$

Each intensity depends on two net phase shifts of two interferometer loops (χ_A etc.). First experimental investigations agree with these predictions [54]. The intensities and interference properties of the loops B and C can partly be controlled by the first interferometer loop. There exist additional positions of

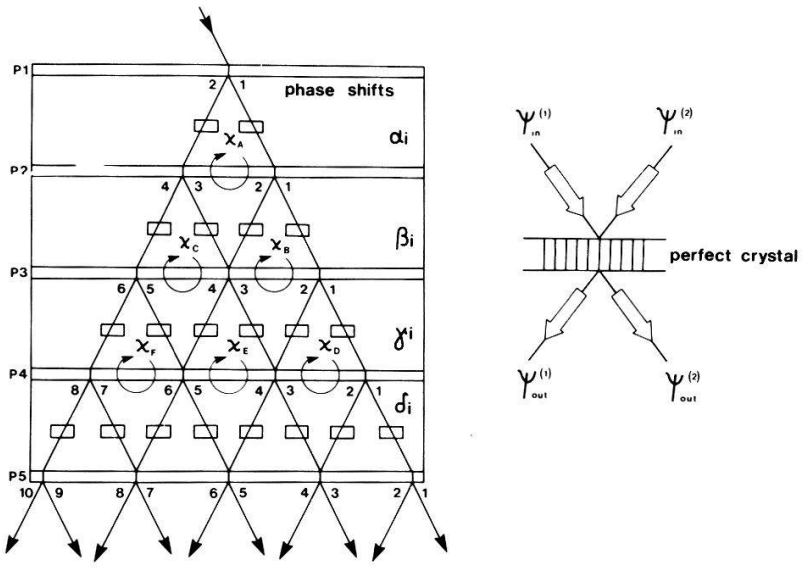

Figure 12
Sketch of a multiplate interferometer with an indication of different interferometer loops (left) and the principle of coherent beam mixing (right).

four-wave mixing, which provide new aspects for coherent neutron optics. The intensities inside these interferometer loops can be coherently influenced not only at the position of the splitter but also at the position of the mirror. This may be useful for the achievement of squeezed neutron states [55] and new bunching systems. The formulas have been checked as to whether a phase shifter can have an influence, if it is placed within a beam with zero intensity (e.g. y_3 if $\chi_A = \pi$). They predict no such influence. Absorbing and thick phase shifters producing phase shifts of the order of the coherence length lead to additional effects.

8. Discussion

All the results of the neutron interferometric experiments are well described by the formalism of quantum mechanics. According to the complementarity principle of the Copenhagen interpretation, the wave picture has to be used to describe the observed phenomena. The question how the well-defined particle properties of the neutron are transferred through the interferometer, is not a meaningful within this interpretation, but it should be an allowed one from the physical point of view. Therefore, other interpretations should also be included in the discussion of such experiments. The particle picture can be preserved if pilot waves are postulated or if a quantum potential guides the particle to the predicted position. Related calculations have been performed for a simplified interfero-

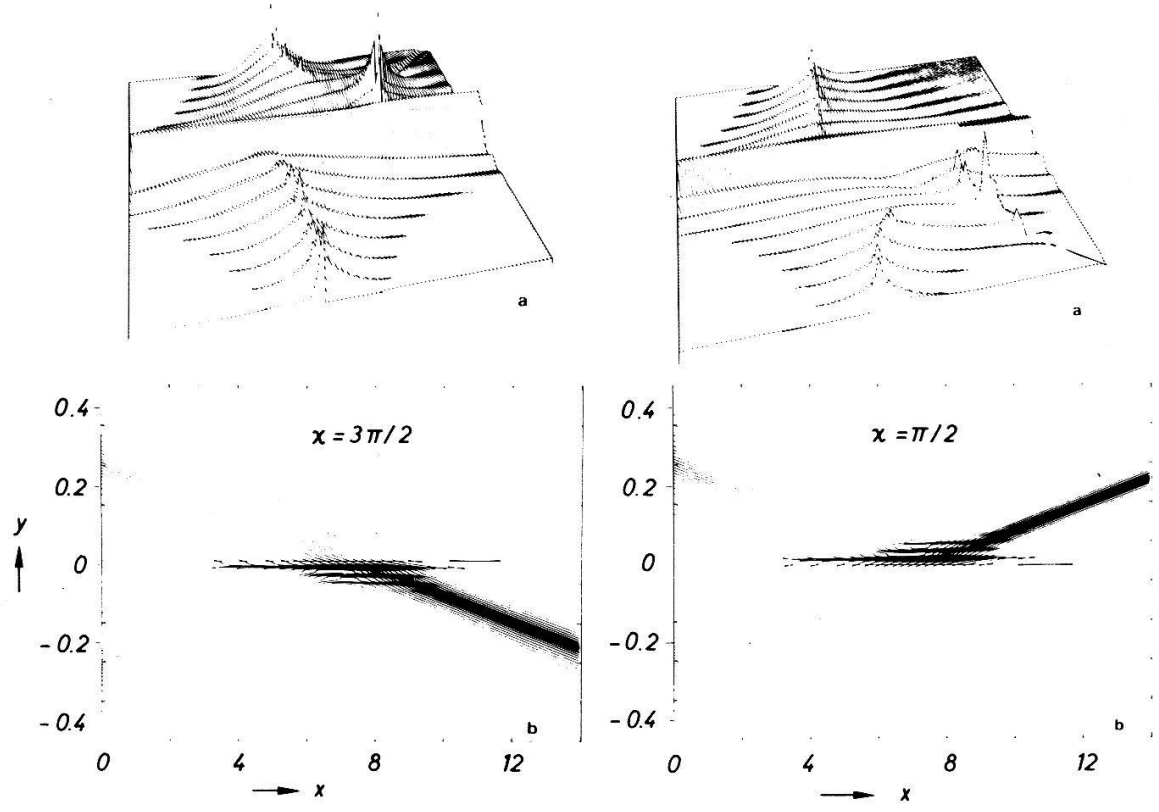

Figure 13
Quantum potential and beam trajectories at the place of beam superposition for a phase shift of $\chi = 3\pi/2$ (left) and $\chi = \pi/2$ (right) [39].

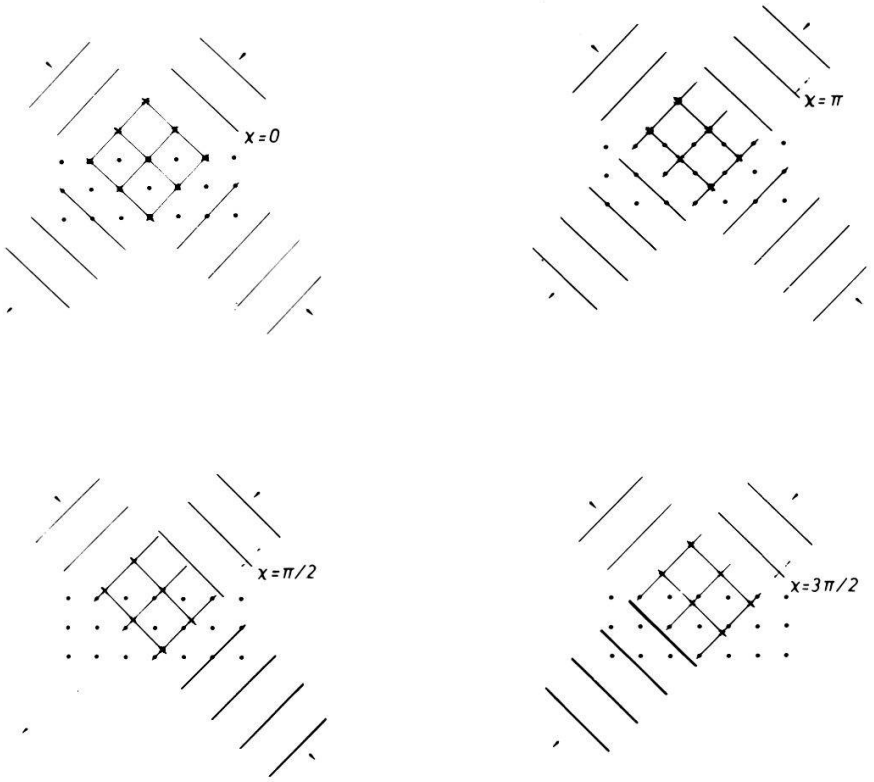

Figure 14
Nodes of the wave field and lattice points at the third interferometer plate. The relative position between the nodes of the wave field and the lattice points depend on the phase shift and determines the beams behind the interferometer.

meter system [39, 40]. The nonlocal quantum potential and the beam trajectories are shown in Fig. 13. The alternative view according to the wave picture is visualised in Fig. 14 where the position of the nodes of the superposed wave fields relative to the lattice points determine where the waves proceed behind the interferometer.

We have always tried to perform unbiased experiments and do not wish to interfere with any epistemological interpretation of quantum mechanics. Perhaps in the future new proposals for experiments will be formulated, which permit a unique decision between different interpretations. As an experimentalist, one appreciates the pioneering work of the founders of quantum mechanics, who created this basic theory with so little experimental evidence. Now we have much more direct evidence, even on a macroscopic scale but, nevertheless, one notices that the interpretation of quantum mechanics goes beyond human intuition in certain cases. Only two aspects of the experiments discussed before should be repeated: How can each neutron in the spin-superposition experiment be transferred from an initial pure state in the $|z\rangle$-direction into a pure state in the $|x\rangle$-direction behind the interferometer, if no spin turn occurs in one beam and a complete spin reversal occurs in the other beam path? How can every neutron have information about which beam to join behind the interferometer, when a slightly different energy exchange occurs in both beams inside the interferometer and the time constant of the beat effect is by many orders of magnitude larger than the time of flight through the system?

Experiments of our group and such which are related to fundamental physics problems have been discussed in this article. Several recent review articles can supplement a broader scope about the status of neutron interferometry [56–59].

Acknowledgment

All the experimental results discussed in detail have been obtained by our Dortmund-Grenoble-Vienna interferometer group working at the high flux reactor in Grenoble. The cooperation within this group and especially the cooperation with colleagues from our Institute, which are cited in the references, is gratefully acknowledged.

REFERENCES

[1] H. MAIER-LEITNITZ and T. SPRINGER, Z. Physik *167* (1962).
[2] R. GAEHLER, J. KALUS and W. MAMPE, J. Phys. *E13* (1980) 546.
[3] H. RAUCH, W. TREIMER and U. BONSE, Phys. Lett. *A47* (1974) 369.
[4] W. BAUSPIESS, U. BONSE, H. RAUCH and W. TREIMER, Z. Physik *271* (1974) 177.
[5] A. I. IOFFE, V. S. ZABIYANKAN and G. M. DRABKIN, Phys. Lett. *111* (1985) 373.
[6] U. BONSE, M. HART, Appl. Phys. Lett. *6* (1965) 155.
[7] H. RAUCH, D. PETRASCHECK, *Neutron Diffraction* (Ed. H. Dachs, Springer Verlag, Berlin 1978) Chap. 9.
[8] V. F. SEARS, Can J. Phys. *56* (1978) 1261.
[9] W. BAUSPIESS, U. BONSE and W. GRAEFF, J. Appl. Cryst *9* (1976) 68.
[10] D. PETRASCHECK, Acta Phys. Austr. *45* (1976) 217.
[11] M. L. GOLDBERGER and F. SEITZ, Phys. Rev. *71* (1947) 294.
[12] V. F. SEARS, Phys. Rep. *82* (1982) 1.
[13] U. BONSE and H. RAUCH (Eds.): *Neutron Interferometry* (Clarendon Press, Oxford 1979).
[14] H. RAUCH, E. SEIDL, D. TUPPINGER, D. PETRASCHECK and R. SCHERM: Z. Physik B (in print).
[15] H. RAUCH and J. SUMMHAMMER, Phys. Lett. *104A* (1984) 44.
[16] J. SUMMHAMMER, H. RAUCH and D. TUPPINGER: Phys. Rev. *A36* (1987) 4447.
[17] Y. AHARONOV and L. SUSSKIND, Phys. Rev. *158* (1967) 1237.
[18] H. J. BERNSTEIN, Phys. Rev. Lett. *18* (1967) 1102.
[19] G. EDER and A. ZEILINGER: Il Nuovo Cim. *34B* (1976) 76.
[20] H. RAUCH, A. ZEILINGER, G. BADUREK, A. WILFING, W. BAUSPIESS and U. BONSE, Phys. Lett. *A54* (1975) 425.
[21] S. A. WERNER, R. COLLELLA, A. W. OVERHAUSER and C. F. EAGEN, Phys. Rev. Lett. *35* (1975) 1053.
[22] A. ZEILINGER, Nature *294* (1981) 544.
[23] H. J. BERNSTEIN, Nature *315* (1985) 42.
[24] H. RAUCH, A. WILFING, W. BAUSPIESS and U. BONSE, Z. Physik *B29* (1978) 281.
[25] M. V. BERRY: Proc. Roy. Soc. London A392 (1984) 45.
[26] J. SUMMHAMMER, G. BADUREK, H. RAUCH, U. KISCHKO and A. ZEILINGER, Phys. Rev. *A27* (1983) 2523.
[27] G. BADUREK, H. RAUCH and J. SUMMHAMMER, Phys. Rev. Lett. *51* (1983) 1015.
[28] A. ZEILINGER, in [13] p. 241.
[29] E. P. WIGNER, Am. J. Phys. *31* (1963) 6.
[30] B. ALEFELD, G. BADUREK and H. RAUCH, Z. Physik *B41* (1981) 231.
[31] G. M. DRABKIN and R. A. ZHITNIKOV, Sov. Phys. JETP*11* (1960) 729.
[32] F. BLOCH and A. SIEGERT, Phys. Rev. *57* (1940) 522.
[33] H. KENDRICK, J. S. KING, S. A. WERNER and A. AROTT, Nucl. Instr. Meth. *79* (1970) 82.
[34] P. CARRUTHERS and M. M. NIETO, Rev. Mod. Phys. *40* (1968) 411.

[35] R. JACKIW: J. Math. Phys. *9* (1968) 339.
[36] R. J. GLAUBER, Phys. Rev. *131* (1963) 2766.
[37] C. DEWDNEY, P. GUERET, A. KYPRIANIDIS and J. P. VIGIER, Phys. Lett. *102A* (1984) 291.
[38] J. P. VIGIER, Pramana *25* (1985) 397.
[39] C. DEWDNEY, Phys. Lett. *109A* (1985) 377.
[40] C. DEWDNEY, P. R. HOLLAND and A. KYPRIANIDIS, Phys. Lett. *A119* (1986) 259.
[41] G. BADUREK, H. RAUCH and D. TUPPINGER, Proc. Int. Conf. *New Techniques and Ideas in Quantum Measurement Theory,* N.Y. Jan. 1986, 133, New York Academy of Science 1986.
[42] G. BADUREK, H. RAUCH and D. TUPPINGER, Phys. Rev. *A34* (1986) 2600.
[43] U. BONSE, W. GRAEFF, R. TEWORTE and R. RAUCH, Phys. stat. sol. (a) *43* (1977) 487.
[44] U. BONSE, W. GRAEFF and H. RAUCH, Phys. Lett. *69A* (1979) 420.
[45] G. M. ALADZHADZHYAN, P. A. BEZIRGANYAN, O. S. SEMERDZHYAN and D. M. VARDANYAN, Phys. stat. sol. (a) *43* (1977) 399.
[46] J. B. M. UFFINK and J. HILGEVOORD, Phys. Lett. *105A* (1984) 176.
[47] D. PETRASCHECK and H. RAUCH, Acta Cryst. *A40* (1984) 445.
[48] H. RAUCH, U. KISCHKO, D. PETRASCHECK and U. BONSE, Z. Physik *B51* (1983) 11.
[49] F. MEZEI (Ed), *Neutron Spin Echo,* Lect. Notes in Physics *128*, Springer 180.
[50] G. BADUREK, H. RAUCH and A. ZEILINGER, in 49) p. 136.
[51] H. RAUCH, in 7) p. 161.
[52] H. KAISER, S. A. WERNER and E. A. GEORGE, Phys. Rev. Lett. *50* (1983) 560.
[53] P. A. BEZIRGANYAN, F. O. EIRAMDSHYAN and K. G. TRUNI, phys. stat. sol. (a) *20* (1973) 611.
[54] M. HEINRICH, D. PETRASCHECK and H. RAUCH, Z. Physik (in preparation).
[55] B. YURKE, Phys. Rev. Lett. *56* (1986) 1515.
[56] A. G. KLEIN and S. A. WERNER: Rep. Progr. Phys. *46* (1983) 259.
[57] D. GREENBERGER, Rev. Mod. Phys. *55* (1983) 875.
[58] H. RAUCH, Contemp. Phys. *27* (1986) 345.
[59] S. A. WERNER and A. G. KLEIN, in "Methods of Experimental Physics" *23*, Part A, 259 Academic Press 1986.